Determination of double-K fracture parameters of concrete using bottom-notched splitting test

Yuan, Wenyan; Dong, Wei; Zhang, Binsheng; Yu, Juyao

Published in:
Journal of Materials in Civil Engineering

DOI:
10.1061/(ASCE)MT.1943-5533.0004737

Publication date:
2023

Document Version
Author accepted manuscript

Determination of double-*K* fracture parameters of concrete by bottom-notched splitting test

Wenyan Yuan[1], Wei Dong[2,*], Binsheng Zhang[3], Juyao Yu[4]

[1]Doctoral student, State Key Laboratory of Coastal and Offshore Engineering, Dalian University of Technology, Dalian 116024, P. R. China. E-mail: yuanwenyan@mail.dlut.edu.cn.

[2]Professor, State Key Laboratory of Coastal and Offshore Engineering, Dalian University of Technology, Dalian 116024, P. R. China.

(*Corresponding author) E-mail: dongwei@dlut.edu.cn

[3]Professor, Department of Civil Engineering and Environmental Management, School of Computing, Engineering and Built Environment, Glasgow Caledonian University, Glasgow G4 0BA, Scotland, United Kingdom. E-mail: Ben.Zhang@gcu.ac.uk

[4]Master student, State Key Laboratory of Coastal and Offshore Engineering, Dalian University of Technology, Dalian 116024, P. R. China. E-mail: yujuyao@mail.dlut.edu.cn.

Abstract

A new fracture test method was proposed in this study to determine the double-K fracture parameters of concrete, named as the bottom-notched splitting (BNS) test. In the BNS test, the concrete cube with a pre-set crack on the bottom surface was subjected to a line compressive load on the top surface. Numerical analyses were first carried out to simulate the stress distributions along the ligament and crack opening profiles of the BNS specimens. Then, the fitting expressions of the stress intensity factor and the crack center opening displacement were derived based on the linear elastic fracture mechanics. A series of BNS tests and three-point bending (TPB) tests with different ratios of the pre-set crack length to the specimen height were conducted to determine the double-K fracture parameters of the concrete. The results indicated that the pre-set cracks in the BNS tests could initiate and propagate throughout the whole cross-sections of the concrete cubes. By substituting the obtained initial fracture loads, maximum loads and critical crack center opening displacements in the BNS tests into the fitting expressions, the double-K fracture parameters could be determined. By comparing with the TPB tests, the BNS tests were proved to be an effective method to determine the double-K fracture parameters of concrete. The BNS tests were convenient to operate and could reduce the damage risk of the pre-set cracks. Meanwhile, they would be also appropriate for assessing the fracture properties of existing concrete structures in service because the cubes would be easily obtained from the samples core-drilled from existing concrete structures.

Keywords: Bottom-notched splitting (BNS), three-point bending (TPB), concrete fracture, stress intensity factor, initial fracture toughness, unstable fracture toughness, critical crack length

Introduction

Various experimental investigations have indicated that the fracture process in quasi-brittle materials, such as concrete, can be divided into three stages, i.e. crack initiation, stable and unstable crack propagations. The crack propagation process in concrete can be analyzed by the *R*-curve method. *R*-curve is the crack propagation resistance curve and describes the quantitative relationship between the crack propagation resistance force and crack length (Bažant and Kazemi 1990, 1991; Ouyang et al. 1990). By contrast, *G*-curves are a series of crack propagation driving curves and describe the quantitative relationship between the crack propagation driving force and crack length. Crack propagation status can be determined by the relationship between the *R*-curve and *G*-curve, including crack initiation, stable and unstable crack propagations. In addition, based on the linear asymptotic superposition assumption, Xu et al. (1999a, b) established the double-*K* fracture model to analyze the crack propagation process of concrete. Besides the traditional unstable fracture toughness, the initial fracture toughness was proposed to reflect the capacity of the concrete material against crack initiation. Taking the initial fracture toughness and unstable fracture toughness as the demarcation points, the crack propagation process of concrete can be distinguished into three stages, i.e. crack initiation, stable crack propagation, and unstable crack propagation. In addition, as an extended application of the double-*K* fracture model, an initial fracture toughness-based crack propagation criterion was proposed and verified by Dong et al. (2013a, b) to analyze the complete fracture process of concrete. At present, the double-*K* fracture model has been widely adopted by researchers to investigate fracture properties of concrete (Dong et al. 2016; Gao et al. 2022; Li et al. 2015; Pradhan et al. 2020; Ruiz et al. 2016) and also recommended as a standard method by RILEM (see RILEM TC265-TDK (2021): Testing methods for determination of the double-*K* criterion for crack propagation in concrete using wedge-splitting tests and three-point bending beam tests) and China Power Industry Standard (see DL/T 5332 (2005) Norm for fracture test of hydraulic concrete).

In general, the double-*K* fracture model is combined with the fictitious crack model (Hillerborg et al. 1976) to characterize the nonlinear fracture behavior of concrete. As the stress intensity factor (SIF) at the pre-set crack tip is greater than the initial fracture toughness, the pre-set crack starts to propagate and the fracture process zone forms. To reflect the cohesive effect induced by the aggregate interlock, the fracture process zone is assumed as an actual crack and the cohesive stress is applied within it. Similar to the *R*-curve method (Bažant and Kazemi 1990, 1991; Ouyang et al. 1990), the crack propagation driving force is the SIF caused by the external load, and the crack propagation resistance is the sum of the SIF caused by the cohesive stress and the initial fracture toughness of the material. Under the maximum load, the SIF caused by the cohesive stress is denoted as the roughness toughness, and the sum of the initial fracture toughness and the roughness toughness is the unstable fracture toughness. The initial fracture toughness is totally based on the linear elastic fracture mechanics. Nevertheless, the unstable fracture toughness considered the cohesive effect within the fracture process zone. In this way, the double-*K* fracture model can be regarded as an improved linear elastic fracture mechanics model, where the nonlinear fracture behavior caused by the aggregate interlock within the fracture process zone is considered.

In the existing investigations, various test methods were utilized by researchers to determine the fracture parameters of concrete, including fracture toughness (Guan et al. 2015; Qing and Cheng 2018), fracture energy (Cifuentes and Karihaloo 2013; Lu and Li 2012; Zhao et al. 2008), and fracture process zone length (Bhowmik and Ray 2019; Hu and Wittmann 1990). The commonly used test methods were three-point bending test, compact tension test, and wedge-splitting test. For the three-point bending test, the test procedure can be implemented easily in a general material laboratory due to the simple experimental set-up (Guan et al. 2016; Lacidogna et al. 2019). At present, the three-point bending test method has been widely used to measure the fracture properties of concrete (Xu and Reinhardt 2000) and other similar materials, e.g. masonry (Wang et al. 2020) and earth blocks (Hall et al. 2022). RILEM recommended the test method using three-point bending beams to determine the fracture parameters of concrete (see RILEM 50-FMC Draft Recommendation (1985) - Determination of the fracture energy of mortar and concrete by means of three-point bend tests on notched beams). However, for large-size concrete beams, the large self-weight would result in additional external loading and cause potential damage at the crack tip during the complete test process (Zhang and Xu 2011). By contrast, the impact of the self-weight can be eliminated in the compact tension test (Ožbolt et al. 2013) and the wedge splitting test (Bakour and Ben 2022; Kumar and Barai 2009). Accordingly, the standard test methods of the compact tension test and wedge splitting test were recommended by ASTM (see ASTM International E399-09 (2009) - Standard test method for linear-elastic plane-strain fracture toughness K_{IC} of metallic materials) and China Power Industry Standard (see DL/T 5332 (2005) Norm for fracture test of hydraulic concrete). It should be noted that both compact tension test and wedge-splitting test require the sophisticated fixtures (Li et al. 2015), which would largely enhance the complexity of the operation and increase the testing cost.

Recent years, the center-notched splitting (CNS) test has been widely utilized by researchers (Hu et al. 2015; Tang et al. 1996) to investigate the fracture properties of concrete. In the CNS test, a vertical crack is pre-set at the center of a cylinder or cube specimen, and the specimen is subjected to line compressive loading along the center lines of both top and bottom surfaces. In this way, the middle cross-section of the specimen is under pure splitting tension and the pre-set crack is under mode-I fracture (Ince 2010, 2012). It was worthy to point out that the center notch is difficult to be made after casting concrete specimens, so that the steel strip is usually fixed in the mold before casting concrete specimens. There would be a potential damage occurring at the crack tip during the pull-out process of the steel strip, resulting in the imprecise experimental results. In addition, for assessing the fracture properties of the concrete structures in service, the CNS test is infeasible because it is difficult to obtain a center notch in the sample core-drilled from the structures. Therefore, it is necessary to provide an effective and simple supplement to the existing test methods for determining the fracture parameters of concrete.

In line with this, a new test method, i.e. the bottom-notched splitting (BNS) test, was proposed and verified in this study. In the BNS test, a vertical crack was pre-set on the bottom surface of a concrete cube, and the concrete cube was subjected to compressive loading along the center line of the top surface with the frictionless contact on the bottom surface. Under this loading condition, the pre-set crack would initiate and propagate until it would penetrate throughout the whole cross-section. Comparing with the traditional three-point bending test and wedge splitting test, the BNS test was convenient to operate and could reduce the damage risk of the pre-set crack. Meanwhile, it was also appropriate to assess the fracture properties of concrete structures in service because the cube would be easy to obtain from the samples core-drilled from existing structures. In addition, the BNS test can be also used to investigate the fracture properties of concrete under multi-axial loading conditions by applying the tensile or compressive loading on other surfaces of the BNS specimen. In this study, numerical analysis was firstly conducted to analyze the mechanical responses of the BNS specimen and then derive the fitting expressions of the stress intensity factor and the crack center opening displacement. Thereafter, the digital image correction (DIC) technique was employed to provide the crack profiles on the surfaces of the BNS specimens with different ratios of the pre-set crack length to the specimen height. Furthermore, a series of BNS tests and three-point bending (TPB) tests were conducted to measure the double-*K* fracture parameters of the concrete including the initial fracture toughness, critical crack length, and unstable fracture toughness. By comparing with the TPB test, the BNS test was proved to be an effective method for determining the double-*K* fracture parameters of concrete.

Loading arrangement of and numerical exploration on the BNS test

Loading arrangement of the BNS test

The BNS specimen was a concrete cube with a vertical crack pre-set on the bottom surface, as shown in Fig. 1(a). The side length of the cube and the length of the pre-set crack were denoted as D and a_0, respectively. In the BNS test, the concrete cube was subjected to a compressive load along the center line of the top surface with the frictionless contact on the bottom surface. To achieve the splitting loading, a steel loading header with a cambered subplate was customized to apply the line load on the top surface, similar to that of the splitting tensile test. According to Chinese Standard (see GB 50081 (2002) - Standard for test method of mechanical properties on ordinary concrete), and the radius of the cambered subplate was 75 mm. In addition, a timber strip with the width of 20 mm and the thickness of 3 mm was placed between the steel loading header and the specimen to avoid local stress concentration and failure near the loading line. To achieve the frictionless contact, three layers of polyvinyl chloride (PVC) films were placed between the bottom surface of the BNS specimen and the lower platform of the testing machine. In particular, the first two layers of PVC films were separated into two identical parts along the pre-set crack to reduce the possible constraint on the crack opening.

All the PVC films were coated with lubricating oil to eliminate the possible friction between the cube specimen and the lower platform of the testing machine. This method has been widely adopted by researchers to eliminate the friction between the concrete specimen and the loading plate (Li et al. 2016, 2018). The loading arrangement of the BNS test is illustrated in Fig. 1(b) and the corresponding mechanical model of the BNS test can be simplified as shown in Fig. 1(c). At present, it is uncertain whether the pre-set crack can initiate and propagate throughout the whole cross-section of the BNS specimen under the loading arrangement.

Compliance calibration of the BNS test

In the BNS test, residual friction constraint existed between the specimen and the lower platform. To investigate the influence of the residual friction constraint on the deformation of the BNS specimen, the compliance calibration with a steel cube was firstly conducted for the BNS test. The steel cube for the compliance calibration is shown in Fig. 2(a). The side length of the steel cube was 100 mm. A vertical crack was set at the bottom of the steel cube using the wire-electrode cutting machine, and the width and length of the vertical crack were 2 mm and 50 mm, respectively. Experimental set-up of the compliance calibration is shown in Fig. 2(b). To measure the external load P, a load cell was connected between the steel loading header and the testing machine. Two knife edges were pasted at the center of the pre-set crack with the scale distance of 20 mm, and a clip gage was mounted between the knife edges to measure the crack center opening displacement *CCOD*. In the BNS test, the displacement-control loading mode was adopted and the loading rate was 0.06 mm/min.

In addition, numerical simulations using finite element software ANSYS 15.0 were carried out to calculate the deformation of the steel cube under the frictionless contact assumption. In the numerical simulations, the three-dimensional specimen was simplified as the plane stress model with the actual thickness. Accordingly, the triangular element Plane 183 was utilized to establish the finite element model of the BNS specimen. A discrete crack was set on the bottom surface of the finite element model to characterize the pre-set crack, as shown in Fig. 3(a). Singular elements were created around the crack tip to reflect the high local stress gradient, as shown in Fig. 3(b). As for the boundary conditions, only vertical constraints were applied on all nodes along the bottom line to reflect the frictionless contact between the BNS specimen and the lower platform. In the numerical analysis, the elastic modulus E and Poisson's ratio v of the steel were 210 GPa and 0.3, respectively.

In the numerical simulations, crack center opening displacements under different external loads were extracted. The comparison of the *P-CCOD* curves between the experimental and numerical results is shown in Fig. 4. It can be seen from the figure that, under the same external load, the experimental crack center opening displacement $CCOD_{\text{exp}}$ values are slightly smaller than the numerical $CCOD_{\text{num}}$ values The small differences between $CCOD_{\text{exp}}$ and $CCOD_{\text{num}}$ may be induced by the residual frictional constraint between the steel cube and the lower platform. Taking the deformation under the external load of 800 kN as an example, $CCOD_{\text{exp}}$ was 27.55 μm and $CCOD_{\text{num}}$ was 28.22 μm, which gave the relative error (R.E.) between them as 2.37%. According to the experimental and numerical results of the compliance calibration, it can be concluded that the residual frictional constraint between the specimen and the lower platform had little influence on the deformation of the BNS specimen. The frictionless contact assumption in the numerical simulations is proved to be reasonable.

Then, numerical simulations were carried out to analyze the stress distribution and crack opening profile of the concrete specimen. In the numerical analysis, the material and geometric parameters were chosen as follows. The elastic modulus E and Poisson's ratio v of the concrete were set as 30 GPa and 0.2, the side length of the BNS specimen, D, and the external load P were set as 100 mm and 30 kN, and the pre-set crack length a_0 values were 20 mm, 30 mm, 50 mm and 70 mm, corresponding to a_0/D = 0.2, 0.3, 0.5 and 0.7, respectively. The element numbers of the finite element models for a_0/D = 0.2, 0.3, 0.5 and 0.7 were 410, 394, 378 and 366. Taking a_0/D = 0.3 as an example, the deformation patterns of the BNS specimen are shown in Figs. 5(a) and (b). By contrast, the deformation patterns of the TPB specimen are shown in Figs. 5(c) and (d). It can be seen that, comparing with the TPB specimen, the crack opening profile of the BNS specimen exhibited the obvious cambered patterns due to the vertical constraints on the bottom surface.

The horizontal stress distributions along the ligament and the crack opening profiles are shown in Figs. 6(a) to (d) for the BNS specimens with a_0/D = 0.2, 0.3, 0.5 and 0.7, respectively. In these figures, the positive and negative values of the horizontal stresses represented the tensile and compressive stresses, respectively. It can be seen from Fig. 6 that, except for the local region near the loading point, the remaining region of the ligament was fully in pure tension. In particular, large stress concentrations occurred at the crack tip for individual conditions. According to the stress-based fracture criterion (Shi et al. 2001; Shi 2004), the crack propagated when the tensile stress reached the tensile strength of the material. Thus, the pre-set crack in the BNS specimen could propagate upward and throughout the whole cross-section, indicating that the BNS test was feasible to investigate the fracture propriety of concrete.

Fitting expressions of the stress intensity factor and crack center opening displacement

For convenient applications, it was necessary to derive an expression of the stress intensity factor (SIF) for the BNS test. According to linear elastic fracture mechanics (LEFM), the stress intensity factor K_I can be defined as follows:

$$K_{\mathrm{I}} = \sigma\sqrt{\pi a} f\left(a/D\right) \tag{1}$$

where a is the crack length, σ is the nominal stress, D is the specimen height along the ligament direction, and $f(a/D)$ is the geometrical function related to the specimen shape. In this study, the SIFs of the BNS specimens were calculated by using the displacement extrapolation method (Wu et al. 2013). To obtain adequate data for the SIFs, a series of numerical analyses were conducted to calculate the SIFs of the BNS specimens, where a_0/D ranged from 0.1 to 0.9 with an interval of 0.1 and D ranged from 100 mm to 500 mm with an interval of 50 mm. By applying the data fitting, the expression for the SIF in MPa·mm$^{1/2}$ was derived as Eq. (2) below:

$$K_{\mathrm{I}} = \frac{P}{D^2}\sqrt{\pi a}\left[0.129 + 0.160\left(a/D\right) + 0.402(a/D)^2 + 0.991(a/D)^3\right] \tag{2}$$

where P is the external load in N, a is the crack length in mm, and D is the side length of the BNS specimen in mm.

In addition, it was necessary to establish a quantitative relationship between the crack opening displacement and the crack length. Because the traditional crack mouth opening displacement *CMOD* was not easy to measure in the BNS tests, the crack center opening displacement *CCOD* was utilized in this study. Similarly, a series of numerical analyses were conducted to extract the *CCOD* values of the BNS specimens, where a_0/D ranged from 0.1 to 0.9 with an interval of 0.1 and D ranged from 100 mm to 500 mm with an interval of 50 mm. By applying the data fitting, the expression for *CCOD* in mm can be derived, as shown in Eq. (3) below:

$$CCOD = \frac{P}{DE}\left[-0.053 + 0.057\exp\left(5.291(a/D)\right)\right] \tag{3}$$

where E is the elastic modulus of concrete in MPa.

To verify the accuracy of Eqs. (2) and (3), the calculation results from the equations were compared with those from the numerical analyses, as shown in Figs. 7(a) and (b). It can be seen that the calculation results showed good agreements with the numerical results, indicating that Eqs. (2) and (3) were accurate for calculating the SIFs and *CCODs* of the BNS specimens with different values of D and a/D. It can be seen from Fig. 7(a) that, with the increase of a_0/D, the K_I values showed an increasing tendency, i.e. $dK_I/da > 0$. This indicated that the BNS specimens proposed in this study was the positive geometry. It should be noted that the derivation of Eq. (3) was totally based on the assumption of LEFM. In fact, the crack would propagate further over an incremental length after the crack initiation, and the fracture process zone would form ahead of the pre-set crack. The cohesive stress acting in the fracture process zone would lead to a nonlinear fracture behavior of concrete. For this reason, the fitting expression based on LEFM, i.e. Eq. (3), would be inaccurate for calculating the crack length of the BNS specimen and need to be corrected further.

Experimental program

Specimen preparations

In the experiment, the side length of the BNS specimen, D, was selected as 100 mm. With the identical cross-section, the specimen dimensions of the TPB specimen were selected as $L \times B \times D$ = 500 mm × 100 mm × 100 mm, where L, B and D represented the length, width and height of the TPB specimens, respectively. The pre-set crack length a_0 values were 20 mm, 30 mm, 50 mm and 70 mm, corresponding to a_0/D = 0.2, 0.3, 0.5 and 0.7, respectively. Ordinary concrete with the strength grade of C30 was adopted in this study, with the mix proportions of cement: water: sand: aggregate = 1: 0.60: 2.01: 3.69 by weight and the maximum aggregate size of 10 mm. The side length of the BNS specimen was at least three times larger than the maximum aggregate size, and hence the concrete for the BNS specimens can be regarded as a homogeneous material. According to the research by Xu and Reinhardt

(1999a, b), for the homogeneous concrete, the double-*K* fracture parameters, i.e. the initial and unstable fracture toughnesses, can be regarded as the material properties and are not affected by the specimen size. Thus, only one specimen size was adopted in this study to investigate the feasibility of the BNS test for determining the double-*K* fracture parameters of concrete.

In the specimen preparation process, the concrete cubes were cast using the standard steel molds and the errors of the specimen sizes were within 1 mm. After casting, a layer of plastic film was used to cover the specimen surface to prevent the internal moisture from evaporation. All the specimens were placed in the laboratory environment for 24 hours after casting and then moved to the curing chamber until the age of 80 days. Basic mechanical properties of concrete at the age of 80 days were determined according the Chinese standard (see GB/T 50081-2002 - Standard for test method of mechanical properties on ordinary concrete). The compressive strength was measured by compression testing on the 150 mm cube specimens, the tensile strength was measured by splitting tension testing on the 150 mm cube specimens as well, and the elastic modulus was measured from compression testing on the prism specimens of 300 mm × 150 mm × 150 mm. The obtained results were shown as follows: the compressive strength was 45.10 MPa, the tensile strength was 3.31 MPa, and the elastic modulus was 33.10 GPa. For both BNS and TPB specimens, the pre-set cracks were cut by using a diamond saw with the 3 mm thick saw blade. The labels of the specimens were denoted as “Specimen type - a_0/D”. For example, “BNS - 0.3” and “TPB - 0.5” represent the BNS specimen with $a_0/D = 0.3$ and the TPB specimen with $a_0/D = 0.5$, respectively.

DIC tests

The digital image correlation (DIC) is an optical, non-contact measurement technique and is able to analyze the displacement field of the specimen surface by comparing the images before and after deformation (Wu et al. 2011). The digital image correlation (DIC) technique has been employed to observe the crack initiation and propagation process of the BNS specimens and would provide straightforward evidence on the failure patterns of the BNS specimens. To create obvious pixels for the image analysis, the speckle patterns were painted on one surface of the BNS specimen by white and black spray paints. The loading components were customized and assembled in a 250 kN closed-loop hydraulic servo-control testing machine (MTS), as shown in Fig. 8(a). The pre-set crack coincided with the axis of the upper device with the monitor of the laser centering instrument. An industrial camera was placed perpendicular to the speckle patterns at the distance of 1.0 m to the specimen. By adjusting the position and focal distance of the camera, the speckle patterns on the specimen surface can be clearly recorded, as shown in Fig. 8(b). The DIC tests were conducted under displacement-control mode at a loading rate of 0.06 mm/min and an image recording rate of 120 images/min.

In the data processing, a computational domain with the area of 50 mm × 70 mm was selected to cover the whole ligament, as shown in Fig. 9. By picking up one computational node from every five pixels in both x and y directions, a node analytical system was extracted to calculate the strain and displacement fields. Based on the node system, a series of analytical lines, i.e. M_0N_0, M_1N_1, M_2N_2, …, M_nN_n, were set with an interval of five pixels. According to the jump points of the horizontal displacements in the analytical lines, the crack profiles and opening displacements can be determined. More details about the data processing of the DIC tests can be found in some previous studies (Wu et al. 2011; Yuan et al. 2021).

BNS tests and TPB tests

The BNS tests were conducted to determine the initial fracture toughness, critical crack length, and unstable fracture toughness of the concrete. The experimental set-up and loading rate were the same as those in the DIC tests. To determine the initial fracture load, two strain gages were pasted horizontally on both sides of the pre-set crack tip with a distance of 5 mm, as shown in Fig. 10(a). When the pre-set crack initiated, the strain energy accumulated near the pre-set crack tip would be released suddenly, leading to large decreases in the strain gage readings. Thus, the initial fracture load can be determined by capturing the turning point on the load - strain (P - ε) curve, as shown in Fig. 10(b). In addition, a clip gage was mounted at the center of the pre-set crack to measure the crack center opening displacement *CCOD*. Moreover, clip gages were mounted along the ligament at an interval of 20 mm from the pre-set crack tip to determine the crack length. Taking specimen BNS-0.3-1 as an example, four clip gages, i.e. C1, C2, C3 and C4, were mounted along the ligament with the distances of 0 mm, 20 mm, 40 mm and 60 mm from the pre-set crack, as shown in Fig. 11(a). In fact, the displacement d values measured by the clip gages consisted of the crack opening displacements and the elastic deformations within the scale distance. At crack initiation status, the crack tip opening displacement was zero, and the opening displacement measured by the clip gage C1 in Fig. 11(a) was just the elastic deformation. In this study, the elastic deformation at crack initiation status, denoted as d_{ini}, was regarded as a standard to judge the cracking status. It was assumed that a certain point along the ligament would be in critical cracking state once the displacement measured by the clip gage reached d_{ini}. In the experiment, the average values of d_{ini} were 13.56 μm, 16.18 μm, 15.80 μm and 15.06 μm for the BNS specimens with a_0/D = 0.2, 0.3, 0.5 and 0.7, respectively. It can be seen that d_{ini} was hardly affected by a_0/D. Thus, the average d_{ini} value of 15.15 μm was adopted to judge the critical cracking status and to further determine the crack length. It has been proved that the displacement d values measured by the clip gages showed a linear distribution along the ligament length (Dong et al. 2022; Yuan et al. 2021). Therefore, the crack length a can be determined by applying the linear interpolation of d_{ini} on the fitting curve for d, as shown in Fig. 11(b).

For comparison, TPB tests were conducted to determine the initial fracture toughness, critical crack length, and unstable fracture toughness of the concrete. The adopted a_0/D values were the same as those in the BNS tests, i.e. a_0/D = 0.2, 0.3, 0.5 and 0.7. The ratio of the supporting span S to the specimen height D was selected as 4, i.e. S/D = 4. Similar to the BNS tests, the loading rate was maintained as 0.06 mm/min and the strain gage method was used to capture the initial fracture load. In addition, two clip gages were used to measure the loading point displacement and the crack mouth opening displacement. Typical TPB specimens and the experimental setup of the TPB test are shown in Figs. 12(a) and (b), respectively.

Results and discussion

Failure patterns of the BNS specimens

In the BNS test, unstable crack propagation occurred suddenly after reaching the maximum load. Thus, there were no perfect descending branches recorded during the BNS tests. Taking the specimens in the DIC tests as examples, the load - crack center opening displacement (P - $CCOD$) curves are shown in Fig. 13 for a_0/D = 0.2, 0.3, 0.5 and 0.7. To demonstrate the failure patterns of the BNS specimens, five stages were selected on the P - $CCOD$ curves and the DIC analyses were conducted to extract the strain fields of these stages. The five stages were distinguished by five loading levels: P_1 (50%P_{max}), P_2 (85%P_{max}), P_3 (98%P_{max}), P_4 (100%P_{max}) and P_5 (98%P_{max} on the descending branch), which are illustrated in Fig. 13. The strain fields by the DIC analyses and the failure patterns in the experiments are shown in Fig. 14 for the BSN specimens with a_0/D = 0.2, 0.3, 0.5 and 0.7.

It can be seen from the strain fields that the pre-set cracks initiated and then propagated upward until they went throughout the whole cross-section, which showed good agreements with the failure patterns in the experiment. In addition, the stable crack propagations before the maximum load were captured for individual conditions. According to the DIC results, the BNS test proposed in this study was strongly verified to be available to determine the fracture properties of concrete.

Initial fracture toughness

According to the determination method shown in Fig. 10(b), the initial fracture load P_{ini} values were determined for both BNS specimens and TPB specimens, as listed in Table 1. Due to the different loading patterns, the values of P_{ini} for the BNS specimens were much larger than those for the TPB specimens. The initial fracture toughness $K_{\text{IC}}^{\text{ini}}$ was the SIF corresponding to the initial fracture load P_{ini} and the pre-set crack length a_0. For the BNS specimens, the equation to calculate $K_{\text{IC}}^{\text{ini}}$ can be derived by substituting P_{ini} and a_0 into Eq. (2) and this is expressed as Eq. (4). The values of $K_{\text{IC}}^{\text{ini}}$ calculated by Eq. (4) are shown in Fig. 15(a), together with their mean values. According to the trend line of the mean values, i.e. the solid line in the figure, it can be concluded that the initial fracture toughness determined by the BNS test was not affected by a_0/D, and this was similar to other previously reported results (Qing et al. 2018; Xu and Reinhardt 1999b).

$$K_{\text{IC}}^{\text{ini}} = \frac{P_{\text{ini}}}{D^2}\sqrt{\pi a_0}\left[0.129 + 0.160\left(a_0/D\right) + 0.402(a_0/D)^2 + 0.991(a_0/D)^3\right] \tag{4}$$

For the TPB tests, the SIF can be calculated by the equation proposed by Xu et al. (2000), as shown in Eq. (5) below:

$$K = \frac{3PS}{2D^2B}\sqrt{a}\,F\left(a/D\right) \tag{5}$$

where P is the external load, S, B and D are the supporting span, width and height of the TPB specimen, and a is the crack length. For $S/D = 4$, the shape function $F(a/D)$ is expressed as Eq. (6) below:

$$F\left(a/D\right)=\frac{1.99-\left(a/D\right)\left(1-\left(a/D\right)\right)\left[2.15-3.93\left(a/D\right)+2.7\left(a/D\right)^{2}\right]}{\left(1+2\left(a/D\right)\right)\left(1-\left(a/D\right)\right)^{3/2}} \tag{6}$$

The initial fracture toughness $K_{\mathrm{IC}}^{\mathrm{ini}}$ of the TPB specimen can be determined by substituting the initial fracture load P_{ini} and the pre-set crack length a_0 into Eq. (5). The comparisons of the $K_{\mathrm{IC}}^{\mathrm{ini}}$ values for the BNS and TPB specimens are shown in Fig. 15(b). It can be seen that the $K_{\mathrm{IC}}^{\mathrm{ini}}$ values determined from the BNS tests showed good agreements with those from the TPB tests, with the relative errors below 10%. It can be concluded that the BNS test was an effective experimental method to determine the initial fracture toughness of concrete.

Critical crack length

The critical crack length a_{c} is a crucial parameter to calculate the unstable fracture toughness. For the BNS specimens, two methods were adopted to determine the critical crack length, i.e. the clip gage method and the DIC method. For the clip gage method, the critical crack length a_{c} can be determined by applying the linear interpolation of $CTOD_{\mathrm{ini}}$ on the fitting curves for w under the maximum load, as listed in Table 1. For the DIC method, the critical crack length a_{c} can be determined from the crack profiles under the maximum loads, as shown in Fig. 16.

In addition, the values of the crack opening displacement u along the ligament are shown in the right side of the figures. According to the crack profiles, the a_{c} values of the BNS specimens with a_0/D = 0.2, 0.3, 0.5 and 0.7 were determined as 43.20 mm, 45.50 mm, 60.89 mm and 80.42 mm, respectively. The critical crack lengths a_{c} values of the BNS specimens are shown in Fig. 17(a). It can be seen that the mean values of a_{c} exhibited an increasing tendency with the increase of a_0/D.

Meanwhile, an explicit expression to calculate the a_{c} values, in mm, of the BNS specimens was derived from Eq. (3), which is expressed as Eq. (7) below:

$$a_{\mathrm{c}}=0.189D\ln\left[\left(17.544\cdot D\cdot E\cdot CCOD_{\mathrm{c}}\right)/P_{\max}+0.930\right] \tag{7}$$

where P_{max} is the maximum load in N, and $CCOD_c$ is the critical crack center opening displacement in mm under the maximum load. The calculated a_c values using Eq. (7) are listed in Table 1, together with the relative errors (REs) between the experimental and analytical results. It can be seen from the table that the calculated a_c values by Eq. (7) were higher than the experimental a_c values by 16.27%, 13.35%, 8.27% and 7.04% for a_0/D = 0.2, 0.3, 0.5 and 0.7, respectively. The slight overestimations by Eq. (7) were mainly resulted from the assumed use of linear elastic fracture mechanics (LEFM) in the derivation process of the expressions. In fact, the crack would propagate further over an incremental length at the maximum load and a cohesive stress could act in the fracture process zone. This would lead to a nonlinear fracture behavior of concrete, so that LEFM could not be appropriate for assessing the critical crack length. With the increase of a_0/D, the ligament length of the BNS specimen decreased and nonlinear behavior of the fracture process became lesser, which resulted in the decreases in the relative errors. It was worthy to point out that, in the two-parameter fracture model proposed by Shah (1990), it was reported that the value of a_c was overestimated by 10-25% with the assumed use of LEFM.

In this study, the ratio of the measured a_c to the calculated one was denoted as the correctional coefficients R_{ac}. It can be seen from Fig. 17(b) that the values of R_{ac} exhibited an approximate linear tendency with a_0/D. The relationship between R_{ac} and a_0/D could be obtained by applying the linear fitting, as expressed in Eq. (8). Furthermore, an improved expression of a_c was proposed by multiplying the correctional coefficient R_{ac} onto Eq. (7), as shown in Eq. (9). The values of a_c calculated by Eq. (9) are shown in Fig. 17(a), together with those from the experiment. It can be seen that the values of a_c determined by the experiment and Eq. (9) showed good agreements, which indicated that Eq. (9) proposed in this study was accurate to calculate the critical crack lengths of the

BNS specimens. It should be noted that the correctional coefficient R_{ac} may be affected by the specimen sizes and the reasonability of Eq. (9) for other specimen sizes need to be further verified.

$$R_{ac} = 0.836 + 0.152\left(a_0/D\right) \tag{8}$$

$$a_c = 0.189D \cdot \ln\left[\left(17.544 \cdot D \cdot E \cdot CCOD_c/P_{max} + 0.930\right)\right] \cdot \left(0.836 + 0.152\left(a_0/D\right)\right) \tag{9}$$

For the TPB specimens, Xu et al. (2000) proposed an analytical expression to calculate the critical crack length a_c, as shown in Eq. (10) below:

$$a_c = \frac{2}{\pi}\left(D + H_0\right)\arctan\sqrt{\frac{B \cdot E \cdot CMOD_c}{32.6P_{max}} - 0.1135} - H_0 \tag{10}$$

where B and D are the width and height of the TPB specimen, H_0 is the thickness of the knife edge, E is the elastic modulus of concrete, and $CMOD_c$ is the critical crack mouth opening displacement under the maximum load. The calculation results of a_c for the TPB specimens are shown in Fig. 16(a). It can be seen that the critical crack lengths of the TPB specimens increase with the increase of a_0/D.

Unstable fracture toughness

The unstable fracture toughness K_{IC}^{un} was the SIF corresponding to the maximum load P_{max} and the critical crack length a_c. For the BNS specimens, the equation to calculate K_{IC}^{un} can be derived by substituting P_{max} and a_c into Eq. (2), which is expressed as Eq. (11). By substituting the measured and calculated a_c values, two distinct values of K_{IC}^{un} could be obtained, denoted as $K_{IC\_Exp.}^{un}$ and $K_{IC\_Cal.}^{un}$, which are listed in Table 1 and shown in Fig. 19(a). It can be seen that the two distinct values of K_{IC}^{un} showed good agreements, with the relative errors below 10%. For the TPB specimens, K_{IC}^{un} can be calculated by substituting P_{max} and a_c into the expression of the SIF, i.e. Eq. (5). For a clear comparison, the mean values of the unstable fracture toughness ($K_{IC\_Cal.}^{un}$) determined by the BNS tests and TPB tests are shown in Fig. 19(b). It can be seen that the K_{IC}^{un} values determined by the BNS tests were hardly affected by a_0/D. According to the existing investigations (Lei et al. 2021; Xu and Reinhardt 1999b;

Zhang and Xu 2011), the unstable fracture toughness can be regarded as a material property and was not affected by the ratio of the pre-set crack length to the specimen height. Thus, it can be concluded that the BNS test can be an effective experimental method to determine the unstable fracture toughness of concrete.

$$K_{\mathrm{IC}}^{\mathrm{un}} = \frac{P_{\max}}{D^2}\sqrt{\pi a_{\mathrm{c}}}\left[0.129 + 0.160\left(a_{\mathrm{c}}/D\right) + 0.402(a_{\mathrm{c}}/D)^2 + 0.991(a_{\mathrm{c}}/D)^3\right] \quad (11)$$

Conclusions

A new test method, named as the bottom-notched splitting (BNS) test, was proposed in this study to determine the double-*K* fracture parameters of concrete. Numerical analyses were firstly conducted to predict the mechanical responses of the BNS specimens. By applying the data fitting method, the fitting expressions of the stress intensity factor and crack center opening displacement of the BNS specimen were derived. Then, the digital image correlation (DIC) technique was employed to explore the crack profiles of the BNS specimens, and a series of the BNS and three-point bending (TPB) tests were conducted to measure the double-*K* fracture parameters of concrete. Based on the numerical analyses and experimental results, the following conclusions can be drawn:

(a) In the BNS test, the concrete cube specimen with a pre-set crack on the bottom surface was subjected to a line compressive load on the top surface with the frictionless contact on the bottom surface. Under this loading form, the pre-set crack would propagate upwards until it went throughout the whole cross-section for the ratios of the pre-set crack length to the specimen height, (a_0/D), ranging from 0.2 to 0.7. Comparing with the traditional test methods, the BNS test was convenient to operate and could reduce the damage risk of the pre-set crack. Meanwhile, it was also appropriate to assess the fracture properties of existing concrete structures in service because the cubes are easy to obtain from the samples core-drilled from existing concrete structures.

(b) Based on linear elastic fracture mechanics, a fitting expression to calculate the stress intensity factor and crack length of the BNS specimen was proposed. By introducing the correction coefficients derived from the experimental results, an improved expression to calculate the critical crack length of the BNS specimen was derived. By substituting the maximum load and critical crack center opening displacement into the expression, the critical crack length in the BNS test can be calculated. The relative errors between the critical crack lengths from the improved expression and experimental detections were within 3.6%, verifying the accuracy of the improved expression.

(c) According to the expressions of the stress intensity factor and critical crack length proposed in this study, the double-*K* fracture parameters, i.e. initial and unstable fracture toughnesses, can be calculated by using the initial fracture load, maximum load, and critical crack center opening displacement. The double-*K* fracture parameters determined by the BNS tests were hardly affected by a_0/D. By comparing with the TPB test, the BNS test was proved to be an effective method to measure the double-*K* fracture parameters of concrete.

Data Availability Statement

All data, models, or codes that support the findings of this study are available from the corresponding author upon reasonable request.

Acknowledgements

The authors gratefully acknowledge the financial support of the National Natural Science

Foundation of China under the grants NSFC 51878117, NSFC 52179123 and NSFC 51979292.

References

Bakour, A., and M. B. Ftima 2022. "Investigation of fracture properties and size effects of mass concrete using wedge splitting tests on large specimens." *Eng. Fract. Mech.* 259: 108144.

Bažant, Z., and M. Kazemi. 1990. "Determination of fracture energy, process zone length and brittleness number from size effect, with application to rock and concrete." *Int. J. Fracture*. 44(2): 111-131.

Bažant, Z., and M. Kazemi. 1991. "Size dependence of concrete fracture energy determined by RILEM work-of-fracture method." *Int. J. Fracture*. 51(2): 121-138.

Bhowmik, S., and S. Ray. 2019. "An experimental approach for characterization of fracture process zone in concrete." *Eng. Fract. Mech.* 211: 401-419.

Cifuentes, H., and B. Karihaloo. 2013. "Determination of size-independent specific fracture energy of normal- and high-strength self-compacting concrete from wedge splitting tests." *Constr. Build. Mater.* 48: 548-553.

Dong, W., W. Yuan, B. Zhang, and H. Zhong. 2022. "Energy-based fracture criterion of rock-concrete interface considering viscoelastic characheristics." *J. Eng. Mech.* 148(2): 04021155.

Dong, W., X. Zhou, and Z. Wu. 2013b. "On fracture process zone and crack extension resistance of concrete based on initial fracture toughness." *Constr. Build. Mater.* 49: 352-363.

Dong, W., X. Zhou, and Z. Wu. 2016. "Fracture mechanisms of rock-concrete interface: Experimental and numerical." *J. Eng. Mech.* 142(7): 04016040.

Dong, W., Z. Wu, and X. Zhou. 2013a. "Calculating crack extension resistance of concrete based on a new crack propagation criterion." *Constr. Build. Mater.* 38: 879-889.

Gao, S., L. Qi, Y. Zhu, and W. Wang. 2022. "Effect of notch depth ratio on mode I and mixed mode I-II fracture properties of engineered cementitious composites (ECC)." *Int. J. Solids Struct.* 236-237: 111363.

Guan, J., Q. Li, Z. Wu, S. Zhao, W. Dong, and S. Zhou. 2015. "Minimum specimen size for fracture parameters of site-casting dam concrete." *Constr. Build. Mater.* 93: 973-982.

Guan, J., X. Hu, and Q. Li. 2016. "In-depth analysis of notched 3-p-b concrete fracture." *Eng. Fract.*

Mech. 165: 57-71.

Hall, E., B. Pulatsu, E. Erdogmus, and B. Skourup. 2022. "Compression, tension, and fracture energy properties of compressed cement-stabilized earth blocks." *Journal of Architectural Engineering*. 28(1): 06021005.

Hillerborg, A., M. Modéer, and P. Petersson. 1976. "Analysis of crack formation and crack growth in concrete by means of fracture mechanics and finite elements." *Cement Concrete Res.* 6(6): 773-781.

Hu, S., X. Zhang, and S. Xu. 2015. "Effects of loading rates on concrete double-*K* fracture parameters." *Eng. Fract. Mech.* 149: 58-73.

Hu, X., and F. Wittmann. 1990. "Experimental method to determine extension of fracture-process zone." *J. Mater. Civil Eng.* 2(1): 15-23.

Ince, R. 2010. "Determination of concrete fracture parameters based on two-parameter and size effect models using split-tension cubes." *Eng. Fract. Mech.* 77(12): 2233-2250.

Ince, R. 2012. "Determination of concrete fracture parameters based on peak-load method with diagonal split-tension cubes." *Eng. Fract. Mech.* 82: 100-114.

Kumar, S., and S. Barai. 2009. "Determining double-K fracture parameters of concrete for compact tension and wedge splitting tests using weight function." *Eng. Fract. Mech.* 76(7): 935-948.

Lacidogna, G., G. Piana, and A. Carpinteri. 2019. "Damage monitoring of three-point bending concrete specimens by acoustic emission and natural frequency analysis." *Eng. Fract. Mech.* 210: 203-211.

Lei, B., H. Li, J. Zuo, H. Liu, M. Yu, and G. Wu. 2021. "Meso-fracture mechanism of Longmaxi shale with different crack-depth ratios: Experimental and numerical investigations." *Eng. Fract. Mech.* 257: 108025.

Li, Q., J. Guan, Z. Wu, W. Dong, and S. Zhou. 2015. "Fracture behavior of site-casting dam concrete." *ACI Mater. J.* 112(1): 11-20.

Li, X., Z. Wu, J. Zheng, H. Liu, and W. Dong. 2018. "Hysteretic bond stress-slip response of deformed bars in concrete under uniaxial lateral pressure." *J. Struct. Eng.* 144(6): 04018041.

Li, X., Z. Wu, J. Zheng, and A. Alahdal. 2016. "Effect of loading rate on bond behavior of deformed reinforcing bars in concrete under biaxial lateral pressures." *J. Struct. Eng.* 142(6): 04016027.

Lu, Y., and Z. Li. 2012. "Study of the relationship between concrete fracture energy and AE signal energy under uniaxial compression." *J. Mater. Civil Eng.* 24(5): 538-547.

Ouyang, C., B. Mobasher, and S. Shah. 1990. "An R-curve approach for fracture of quasi-brittle materials." *Engineering Fracture Mechanics*. 37(4): 901-913.

Ožbolt, J., J. Bošnjak, and E. Sola. 2013. "Dynamic fracture of concrete compact tension specimen: Experimental and numerical study." *Int. J. Solids Struct.* 50(25-26): 4270-4278.

Pradhan, S., S. Kumar, and S. Barai. 2020. "Impact of particle packing method of design mix on fracture behavior of concrete: Critical analysis." *J. Mater. Civil Eng.* 32(4): 04020045.

Qing, L., M. Dong, and J. Guan. 2018. "Determining initial fracture toughness of concrete for split-tension specimens based on the extreme theory." *Eng. Fract. Mech.* 189: 427-438.

Qing, L., and Y. Cheng. 2018. "The fracture extreme theory for determining the effective fracture toughness and tensile strength of concrete." *Theor. Appl. Fract. Mec.* 96: 461-467.

Ruiz, G., J. Ortega, R. Yu, S. Xu, and Y. Wu. 2016. "Effect of size and cohesive assumptions on the double-*K* fracture parameters of concrete." *Eng. Fract. Mech.* 166: 198-217.

Shah, S. 1990. "Determination of fracture parameters (K^{s}_{IC} and $CTOD_{c}$) of plain concrete using three-point bend tests." *Mater. Struct.* 23(6): 457-460.

Shi, Z. 2004. "Numerical analysis of mixed-mode fracture in concrete using extended fictitious crack model." *J. Struct. Eng.* 130(11): 1738-1747.

Shi, Z., M. Ohtsu, M. Suzuki, and Y. Hibino. 2001. "Numerical analysis of multiple cracks in concrete using the discrete approach." *J. Struct. Eng.* 127(9): 1085-1091.

Tang, T., Z. Bažant, S. Yang, and D. Zollinger. 1996. "Variable-notch one-size test method for fracture energy and process zone length." *Eng. Fract. Mech.* 55(3): 383 – 404.

Wang, B., X. Hu, and P. Lu. 2020. "Modelling and testing of large-scale masonry elements under three-point bending – Tough and strong nacre-like structure enlarged by a factor of 20,000." *Eng. Fract. Mech.* 229: 106961.

Wu, Z., H. Rong, J. Zheng, F. Xu, and W. Dong. 2011. "An experimental investigation on the FPZ properties in concrete using digital image correlation technique." *Eng. Fract. Mech.* 78(17): 2978-2990.

Wu, Z., H. Rong, J. Zheng, and W. Dong. 2013. "Numerical method for mixed-mode I-II crack propagation in concrete." *J. Eng. Mech.* 139(11): 1530-1538.

Xu, S., and H. Reinhardt. 1999a. "Determination of double-*K* criterion for crack propagation in quasi-brittle fracture, Part I: Experimental investigation of crack propagation." *Int. J. Fracture*. 98(2): 111-149.

Xu, S., and H. Reinhardt. 1999b. "Determination of double-*K* criterion for crack propagation in quasi-brittle fracture, Part II: Analytical evaluating and practical measuring methods for three-point bending notched beams." *Int. J. Fracture*. 98(2): 151-177.

Xu, S., and H. Reinhardt. 2000. "A simplified method for determining double-*K* fracture parameters for three-point bending tests." *Int. J. Fracture*. 104(2): 181-209.

Yuan, W., W. Dong, B. Zhang, and H. Zhong. 2021. "Investigations on fracture properties and analytical solutions of fracture parameters at rock-concrete interface." *Constr. Build. Mater.* 300(3): 124040.

Zhang, X., and S. Xu. 2011. "A comparative study on five approaches to evaluate double-*K* fracture toughness parameters of concrete and size effect analysis." *Eng. Fract. Mech.* 78(10): 2115-2138.

Zhao, Z., S. Kwon, and S. Shah. 2008. "Effect of specimen size on fracture energy and softening curve of concrete: Part I. Experiments and fracture energy." *Cement Concrete Res.* 38(8): 1049-1060.

Table 1 Experimental results of the BNS tests and TPB tests

Bottom-notched splitting (BNS) tests									**Three-point bending (TPB) tests**					
Specimen	P_{ini}	$P_{\max}$	a_c (mm) and RE (%)			SIF (MPa·m$^{1/2}$) and RE (%)			Specimen	P_{ini}	$P_{\max}$	a_c (mm)	SIF (MPa·m$^{1/2}$)	
	(kN)	(kN)	Exp.	Eq. (7) (RE)	Eq. (9) (RE)	K_{IC}^{ini}	$K_{IC\_Exp.}^{un}$	$K_{IC\_Cal.}^{un}$ (RE)		(kN)	(kN)	Eq. (5)	K_{IC}^{ini}	K_{IC}^{un}
BNS-0.2-1	110.16	115.41	39.23	44.98 (14.66)	38.97 (0.66)	0.51	1.27	1.26 (1.09)	TPB-0.2-1	3.55	4.43	46.74	0.53	1.36
BNS-0.2-2	109.23	121.09	40.56	49.86 (22.93)	43.20 (6.51)	0.51	1.41	1.57 (11.69)	TPB-0.2-2	3.50	5.10	40.49	0.52	1.30
BNS-0.2-DIC	99.04	102.61	43.20	48.05 (11.23)	41.63 (3.63)	0.46	1.33	1.25 (6.04)	TPB-0.2-3	3.62	4.44	48.00	0.54	1.42
Mean	**106.14**	**113.04**	**41.00**	**47.63 (16.27)**	**41.27 (3.60)**	**0.49**	**1.34**	**1.36 (6.27)**	**Mean**	**3.56**	**4.66**	**45.08**	**0.53**	**1.36**
BNS-0.3-1	76.08	91.31	45.50	50.51 (11.01)	44.53 (2.13)	0.56	1.31	1.25 (4.20)	TPB-0.3-1	2.81	3.75	48.92	0.54	1.22
BNS-0.3-2	69.36	85.61	48.46	55.94 (15.44)	49.32 (1.77)	0.51	1.38	1.43 (3.67)	TPB-0.3-2	2.91	4.15	48.03	0.56	1.32
BNS-0.3-DIC	59.83	69.66	55.93	63.54 (13.61)	56.02 (0.16)	0.44	1.51	1.52 (0.43)	TPB-0.3-3	2.70	3.84	49.00	0.52	1.25
Mean	**68.42**	**82.19**	**49.96**	**56.66 (13.35)**	**49.95 (1.35)**	**0.50**	**1.40**	**1.40 (2.77)**	**Mean**	**2.81**	**3.91**	**48.65**	**0.54**	**1.26**
BNS-0.5-1	26.79	39.77	60.89	66.38 (9.02)	60.54 (0.58)	0.46	1.04	1.03 (1.10)	TPB-0.5-1	1.64	2.03	63.17	0.55	1.11
BNS-0.5-2	38.86	51.53	61.97	66.21 (6.84)	60.38 (2.56)	0.67	1.41	1.33 (6.03)	TPB-0.5-2	1.68	2.28	59.25	0.57	1.06
BNS-0.5-DIC	29.05	44.75	66.56	72.51 (8.94)	66.13 (0.65)	0.50	1.44	1.42 (1.25)	TPB-0.5-3	1.66	2.17	61.17	0.56	1.09
Mean	**31.57**	**45.35**	**63.14**	**68.36 (8.27)**	**62.35 (1.26)**	**0.54**	**1.30**	**1.26 (2.79)**	**Mean**	**1.66**	**2.16**	**61.20**	**0.56**	**1.09**
BNS-0.7-1	12.66	22.90	83.65	87.56 (4.67)	82.52 (1.35)	0.46	1.32	1.27 (3.58)	TPB-0.7-1	0.84	0.91	78.34	0.55	1.10
BNS-0.7-2	14.82	27.20	81.59	84.56 (3.64)	79.69 (2.33)	0.54	1.47	1.38 (6.19)	TPB-0.7-2	0.88	0.95	77.36	0.58	1.08
BNS-0.7-DIC	19.36	22.99	80.42	90.73 (12.82)	85.50 (6.32)	0.71	1.19	1.41 (18.07)	TPB-0.7-3	0.74	0.81	80.26	0.48	1.13
Mean	**15.61**	**21.70**	**81.89**	**87.62 (7.04)**	**82.57 (3.44)**	**0.57**	**1.33**	**1.35 (9.28)**	**Mean**	**0.82**	**0.89**	**78.65**	**0.54**	**1.10**

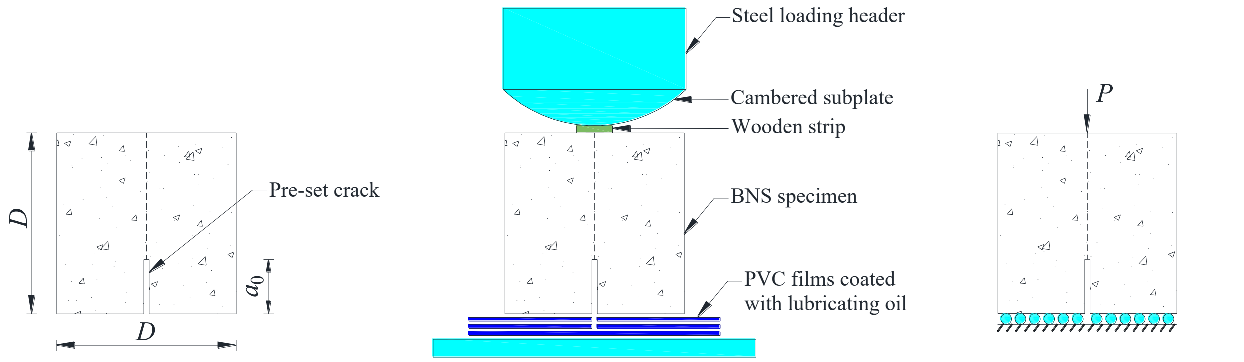

(a) BNS specimen (b) Loading arrangement (c) Mechanical model

Fig. 1 Arrangement of the BNS test and the mechanical modeling

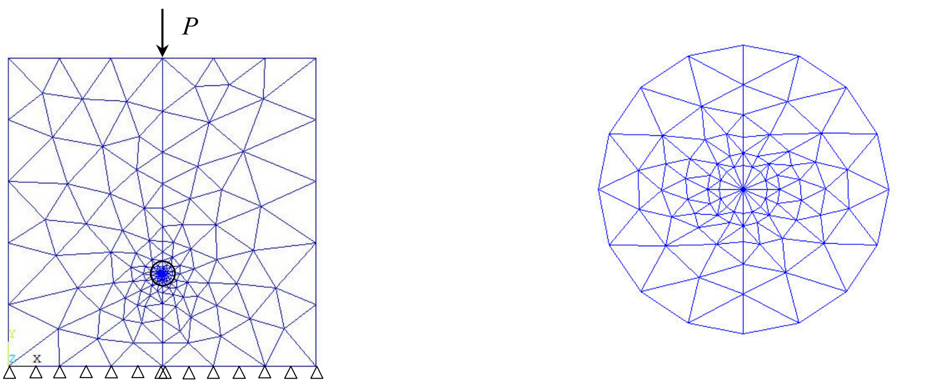

(a) Overall model (b) Local model of crack tip

Fig. 2 Finite element model of the BNS test

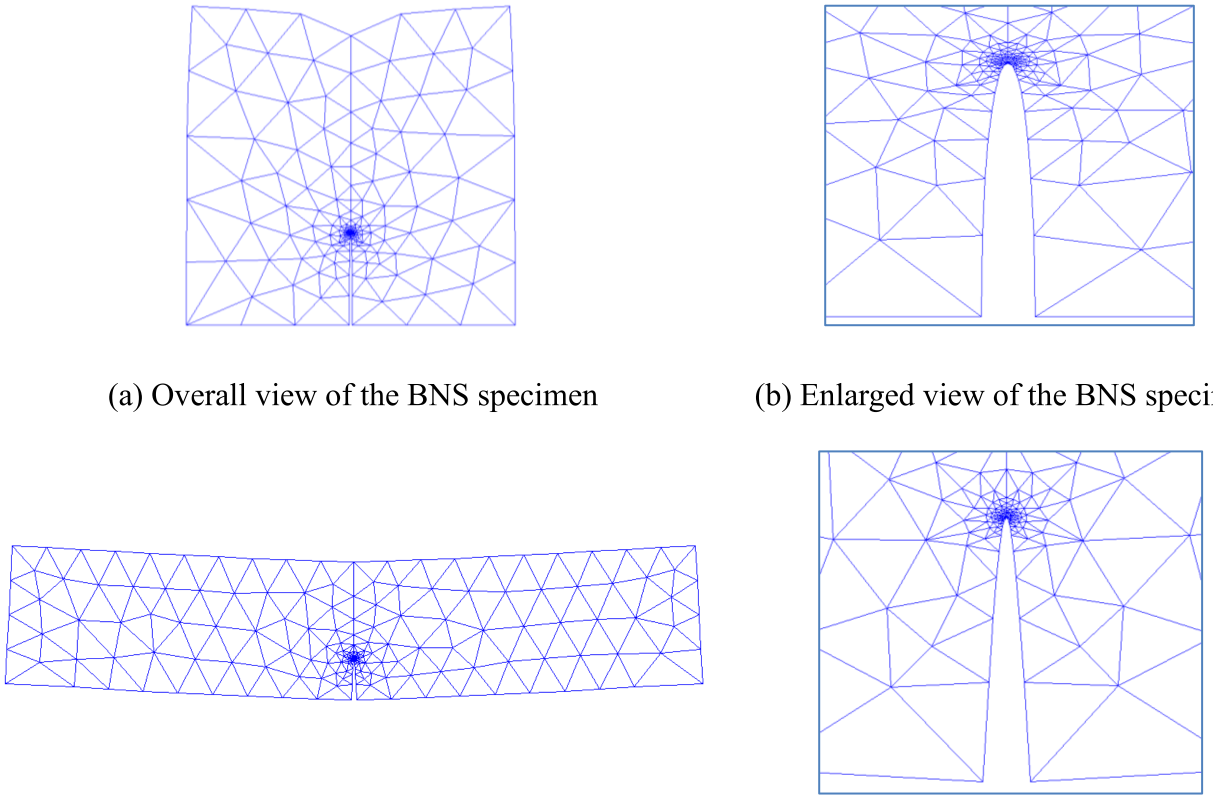

(a) Overall view of the BNS specimen (b) Enlarged view of the BNS specimen

(c) Overall view of the TPB specimen (d) Enlarged view of the TPB specimen

Fig. 3 Deformation patterns of the BNS and TPB specimens

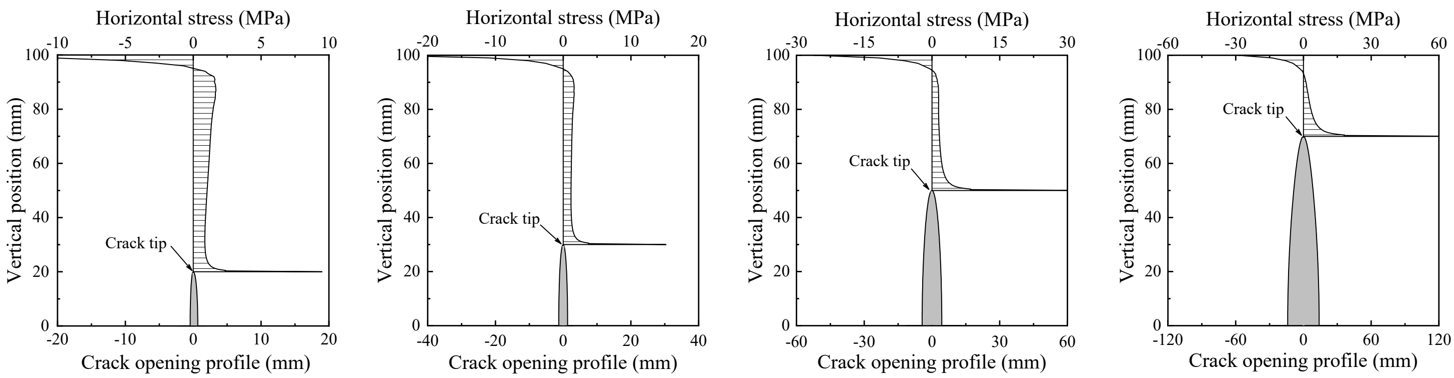

(a) $a_0/D = 0.2$ (b) $a_0/D = 0.3$ (c) $a_0/D = 0.5$ (d) $a_0/D = 0.7$

Fig. 4 Horizontal stress distributions along the ligament and crack opening profiles of the BNS specimens

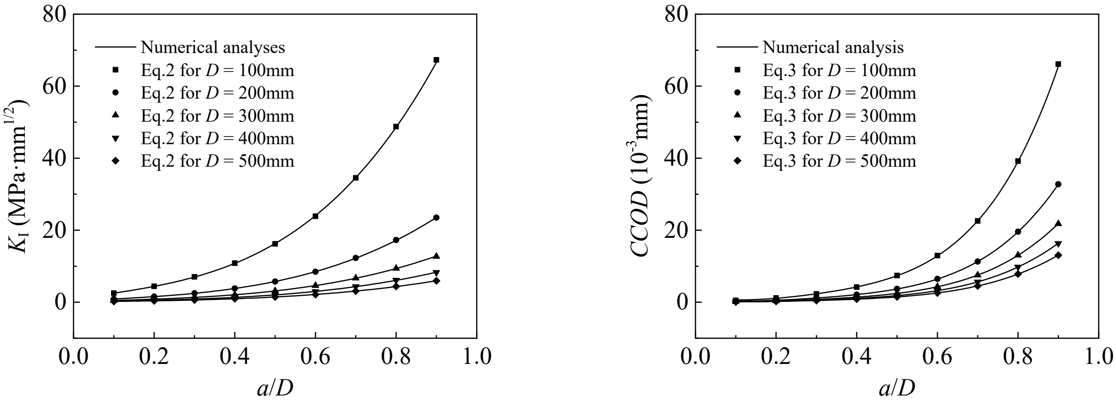

(a) SIF versus a/D (b) $CCOD$ versus a/D

Fig. 5 Comparisons of the SIFs and *CCODs* between the fitting expressions and numerical analyses

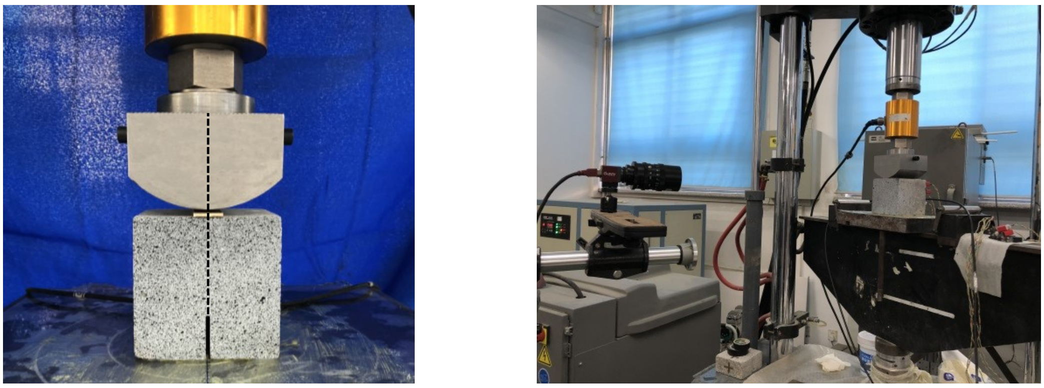

(a) Loading components (b) Experimental set-up

Fig. 6 DIC test on the BNS specimen

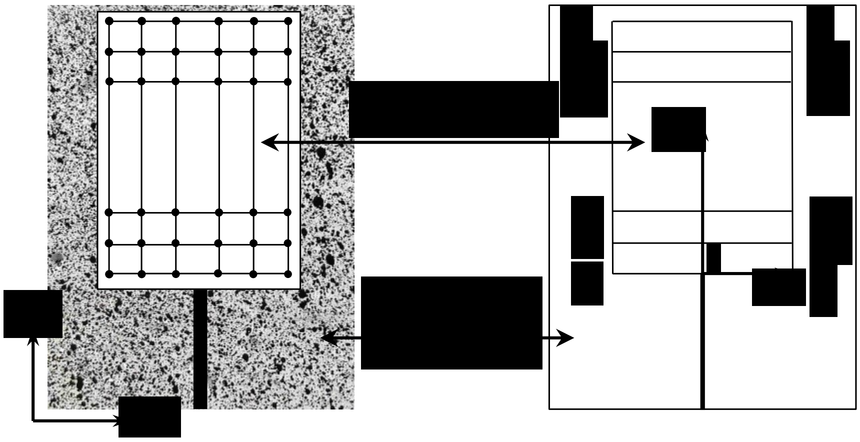

Fig. 7 Computational domain of BNS - 0.3 - DIC specimen

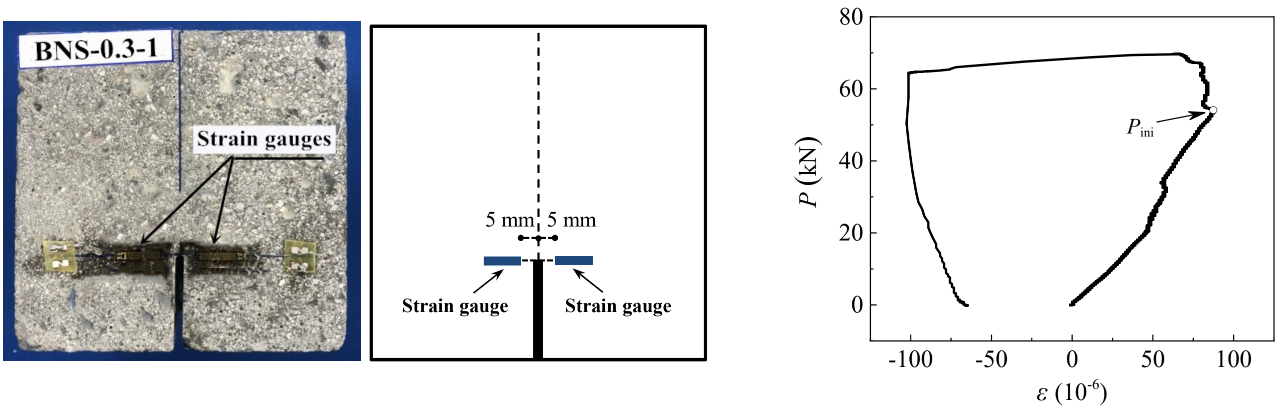

(a) Arrangement of strain gages (b) Determination method

Fig. 8 Determination of the initial fracture load in the BNS test

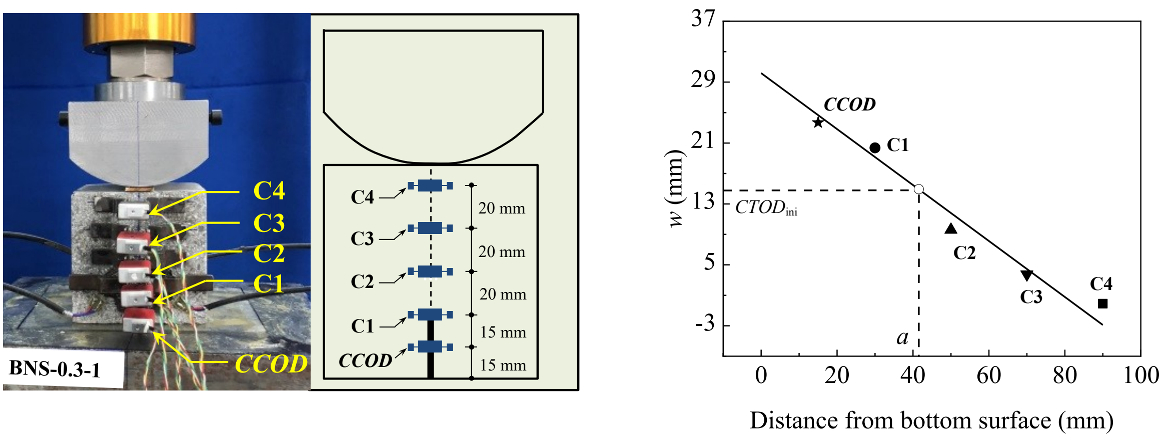

(a) Arrangement of clip gages (b) Determination method

Fig. 9 Determination of the crack length in the BNS test

(a) Typical TPB specimens (b) Experimental set-up of the TBB test

Fig. 10 Typical TBS specimens and the set-up of the TPB test

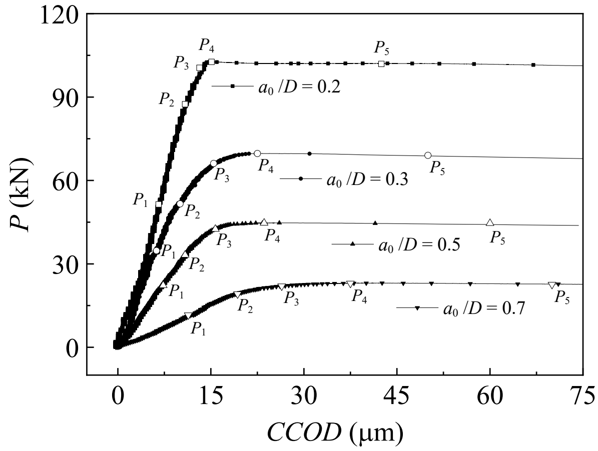

Fig. 11 P - $CCOD$ curves of the BNS specimens

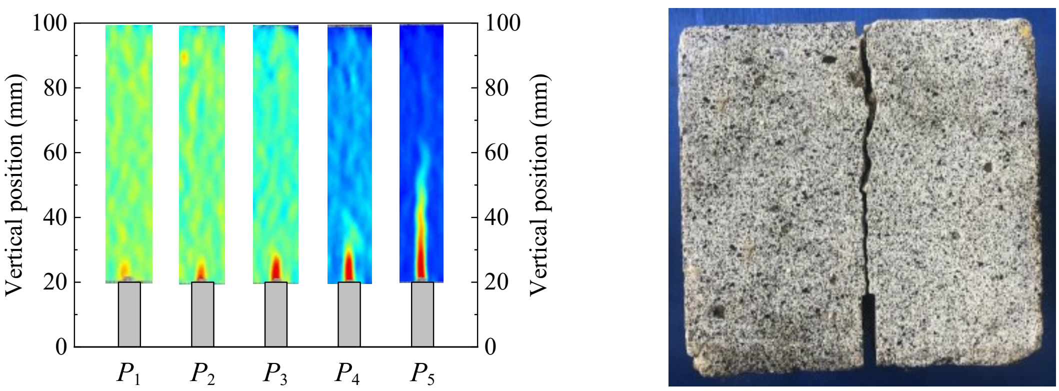

(a) Strain fields for $a_0/D = 0.2$ (b) Failure pattern for $a_0/D = 0.2$

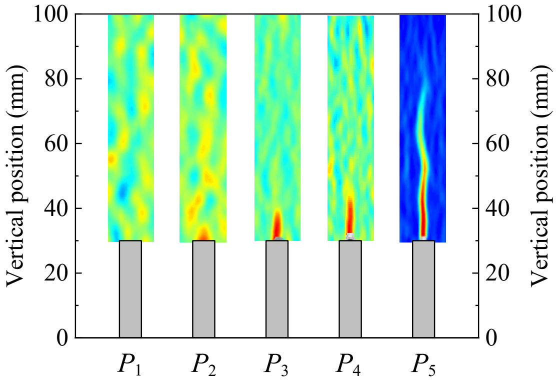

(c) Strain fields for $a_0/D = 0.3$ (d) Failure pattern for $a_0/D = 0.3$

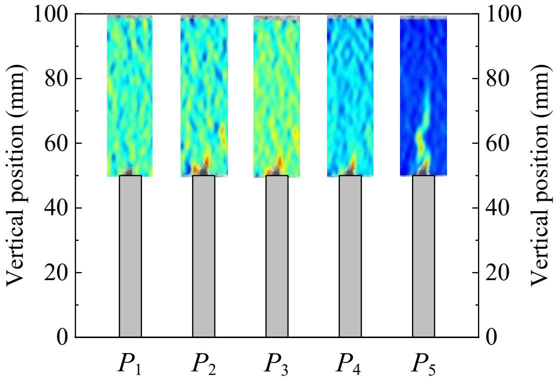

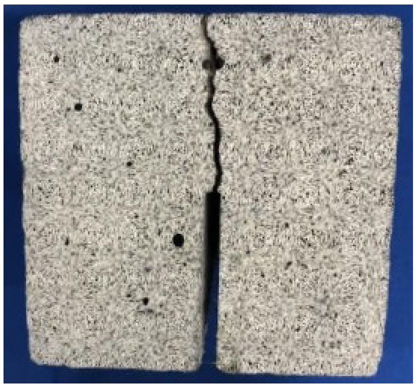

(e) Strain fields for $a_0/D = 0.5$ (f) Failure pattern for $a_0/D = 0.5$

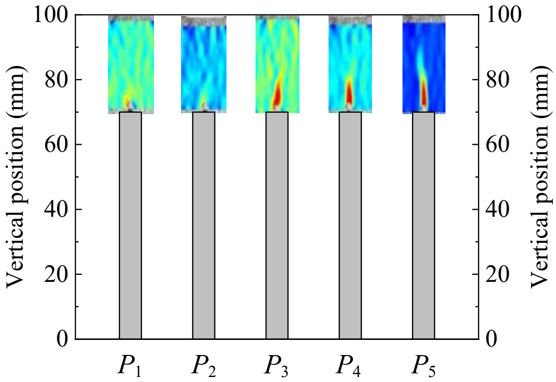

(g) Strain fields for $a_0/D = 0.7$ (h) Failure pattern for $a_0/D = 0.7$

Fig. 12 Strain fields and failure patterns of the BNS specimens with different a_0/D values

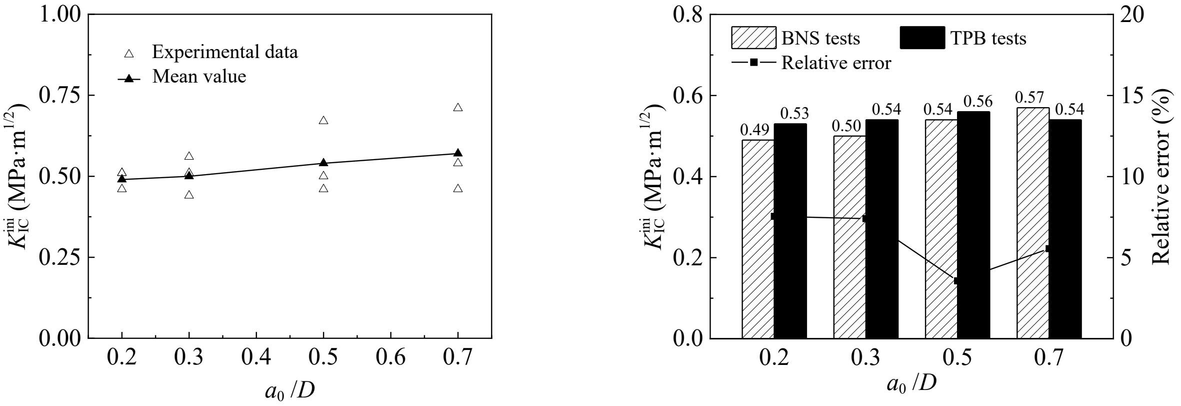

(a) K_{IC}^{ini} determined by the BNS test (b) Comparisons of the K_{IC}^{ini} values

Fig. 13 Initial fracture toughness K_{IC}^{ini} determined by the BNS and TPB tests

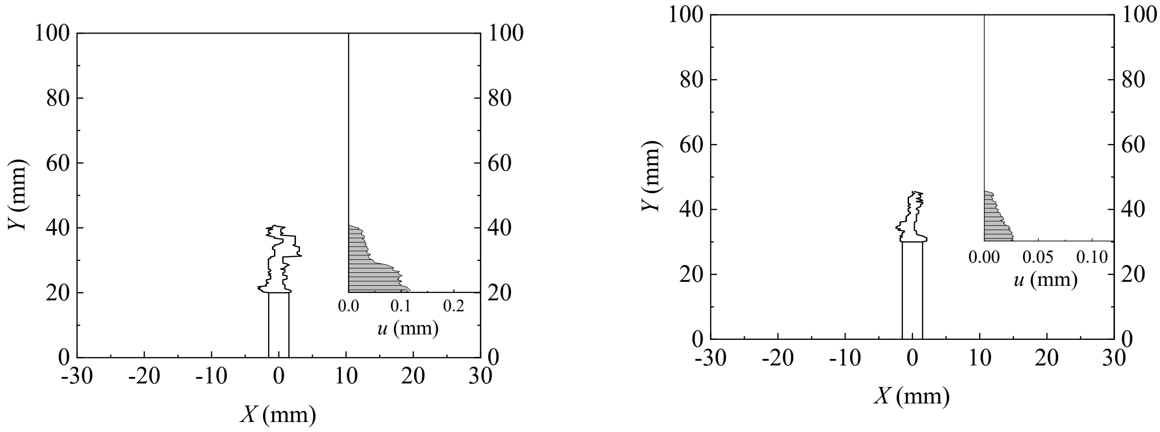

(a) $a_0/D = 0.2$ (b) $a_0/D = 0.3$

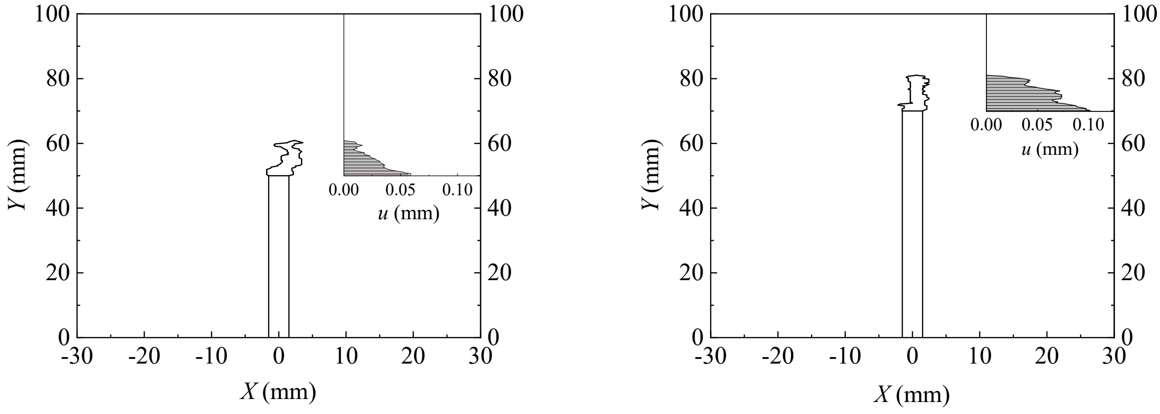

(c) $a_0/D = 0.5$ (d) $a_0/D = 0.7$

Fig. 14 Crack profiles of the BNS specimens under the maximum load

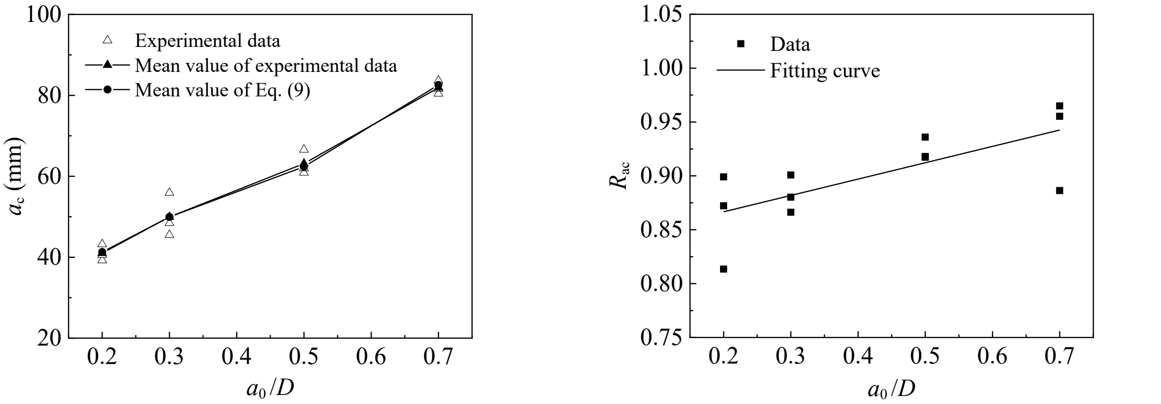

(a) Critical crack length a_c versus a_0/D (b) Correctional coefficient R_{ac} versus a_0/D

Fig. 15 Critical crack length a_c and the correctional coefficient R_{ac} versus a_0/D

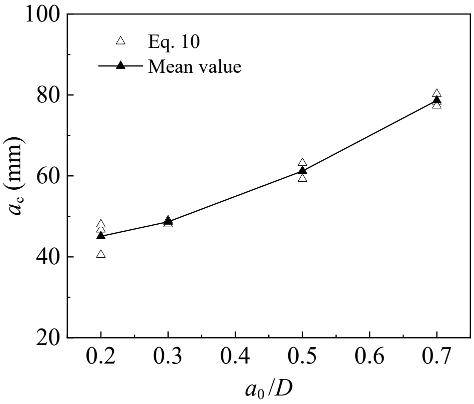

Fig. 16 Critical crack lengths from the TPB tests

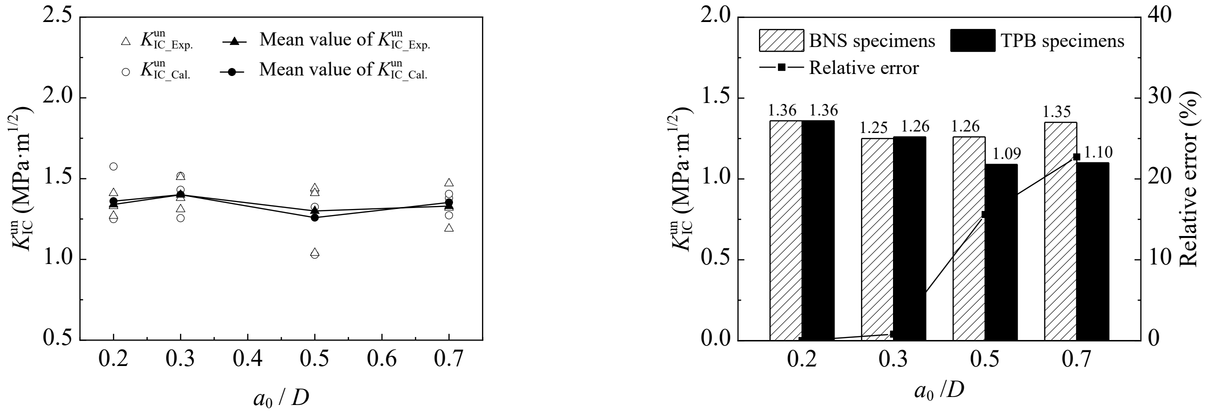

(a) K^{un}_{IC} versus a_0/D for the BNS tests (b) Comparisons of the K^{un}_{IC} values from the BNS and TPB tests

Fig. 17 Unstable fracture toughness K^{un}_{IC} values determined by the BNS and TPB tests